Drug Design, Development and Therapy

Dovepress
Taylor & Francis Group

Open Access Full Text Article

ORIGINAL RESEARCH

Artesunate Mitigates Sepsis-Induced Acute Kidney Injury via Lactate/AMPK/mTOR-Regulated Autophagy Based on Multi-Omics

Hetao Chen[1,*], Peipei Du[1,*], Ran Guo[1], Xuejiao Li[2], Lei Zhang[3], Jiajia Duan[1], Menglu Chen[1], Jia Guo[1], Ying Li[4], Tao Jiang[1]

[1]Department of Clinical Laboratory, The First Affiliated Hospital, and College of Clinical Medicine of Henan University of Science and Technology, Luoyang, People's Republic of China; [2]Henan Key Laboratory of Rare Diseases, Endocrinology and Metabolism Center, The First Affiliated Hospital, and College of Clinical Medicine of Henan University of Science and Technology, Luoyang, People's Republic of China; [3]Department of Integrative Medicine, The First Affiliated Hospital, and College of Clinical Medicine of Henan University of Science and Technology, Luoyang, People's Republic of China; [4]Department of Pharmacy, The First Affiliated Hospital, College of Clinical Medicine of Henan University of Science and Technology, Luoyang, People's Republic of China

*These authors contributed equally to this work

Correspondence: Ying Li; Tao Jiang, Email liying13552@163.com; jiangtao_jyk@126.com

Background: Sepsis-induced acute kidney injury (S-AKI) is a form of acute renal failure resulting from a systemic inflammatory response triggered by infection, and has emerged as a significant public health challenge. Prior studies have demonstrated that artesunate (ART) exerts therapeutic effects on S-AKI by mitigating inflammation and oxidative stress. However, the precise regulatory mechanisms remain to be fully elucidated.

Methods: This study investigates the impact of ART on renal function in a sepsis mouse model and its effect on LPS-induced cytotoxicity in HK-2 cells, aiming to clarify the potential therapeutic mechanisms underlying ART's efficacy in S-AKI. We evaluated changes in body weight, kidney index, biochemical markers, and histopathological alterations in mice, as well as proliferation and apoptosis in HK-2 cells. Additionally, metabolomics and transcriptomics were employed to identify key pathways involved in ART's therapeutic actions.

Results: Our findings indicate that ART significantly improves renal function in sepsis mice, evidenced by increased body weight, reduced kidney index, and diminished pathological damage. Furthermore, ART alleviates LPS-induced cytotoxicity in HK-2 cells, reduce the levels of pro-inflammatory cytokines IL-1β, IL-6, and TNF-α, and increase the levels of antioxidant GSH. Integrative analysis of metabolomics and transcriptomics reveals that ART intervention markedly decreases lactate levels, inhibits excessive AMPK activation, relieves mTOR pathway suppression, and suppresses excessive autophagy, thereby attenuating inflammation and oxidative stress, and mitigating renal cell injury.

Conclusion: The findings suggest that ART may mitigate inflammation and oxidative stress while improving renal function in S-AKI by modulating the lactate/AMPK/mTOR pathway and inhibiting excessive autophagy.

Keywords: acute kidney injury, artesunate, multi-omics, lactate/AMPK/mTOR pathway, autophagy

Introduction

Sepsis is a multi-organ dysfunction syndrome resulting from a dysregulated host response to infection, with acute kidney injury (AKI) being one of its most frequent and severe complications.[1–3] Approximately 60% of sepsis patients develop acute kidney injury (AKI),[4,5] and the presence of this complication markedly increases the mortality risk in sepsis patients. The mortality rate for sepsis patients with AKI is 2 to 3 times higher than that for patients without AKI.[6] Therefore, sepsis-induced AKI (S-AKI) has emerged as a significant global public health challenge.[7,8] Current treatment strategies for S-AKI primarily involve broad-spectrum antibiotics and fluid resuscitation to prevent multi-organ failure, including kidney failure.[9,10] However, these

Received: 24 March 2025
Accepted: 20 June 2025
Published: 10 July 2025

interventions have not yet substantially improved clinical outcomes for patients.[11] Consequently, there is an urgent need to identify new therapeutic targets and approaches to enhance renal function and improve survival in patients with sepsis.

Artemisinin, the primary active ingredient of the traditional Chinese herbal plant *Artemisia annua L*., has demonstrated therapeutic potential in treating chronic and refractory diseases and may hold significant promise for the development of modern medicines.[12] Artesunate (ART), an artemisinin derivative isolated from artemisinin, exhibits superior efficacy and stability compared to artemisinin.[13] Recent studies have demonstrated that ART can exert organ and tissue protective effects by modulating oxidative stress, inflammation, autophagy, apoptosis, and fibrosis,[14,15] suggesting its potential therapeutic benefits for sepsis and associated AKI. Studies have demonstrated that ART can mitigate high glucose-induced damage in rat glomerular mesangial cells by inhibiting inflammatory responses, oxidative stress, and extracellular matrix accumulation.[16] In addition, ART has been reported to attenuate cisplatin-induced acute kidney injury by inhibiting oxidative stress and inflammation.[17] At present, the specific mechanisms by which ART exerts its effects in the treatment of sepsis-induced AKI are not fully understood. Consequently, exploring the mechanisms of ART in treating S-AKI holds significant scientific and clinical value.

With the rapid advancement of high-throughput sequencing and mass spectrometry technologies, transcriptomics and metabolomics have emerged as integral components of systems biology, offering novel insights into the mechanisms of drug action.[18,19] Transcriptomics, through the analysis of gene expression profiles, elucidates how drugs regulate gene transcription, thereby providing critical clues for identifying potential drug targets.[20,21] Metabolomics, by monitoring changes in intracellular and extracellular metabolites, directly reflects the physiological responses to drug interventions, offering comprehensive metabolic-level evidence for pharmacological studies.[22–25] The integration of these two approaches enables a holistic and systematic dissection of drug-induced molecular mechanisms at both transcriptional and metabolic levels.[26,27] This multi-omics strategy not only overcomes the limitations of single-omics analyses but also enhances the precision in uncovering key pathways and targets, thus providing robust support for new drug discovery, efficacy optimization, and toxicity assessment. Therefore, this study employed an integrated approach combining metabolomics and transcriptomics to investigate the molecular mechanisms underlying ART in the treatment of S-AKI. Extensive evidence has demonstrated that ART can modulate transcriptional and metabolic networks via multiple targets, thereby exhibiting broad-spectrum therapeutic potential. For instance, in a diabetes model, artesunate was found to enhance the expression of the glucose transporter GLUT2 by upregulating the phosphorylation levels of PI3K and Akt proteins. Furthermore, it effectively corrected metabolic imbalances in amino acids, lipids, purines, and bile acids, consequently ameliorating abnormal glucose and lipid metabolism.[28] In obesity treatment, artesunate activates the integrated stress response (ISR), leading to the induction of the transcription factor CHOP. This subsequently results in a significant upregulation of hepatic GDF15 expression, which interacts with the GFRAL receptor to form the GDF15/GFRAL signaling axis, thereby suppressing appetite and reducing energy intake.[29] The pleiotropic effects of ART in regulating transcriptional and metabolic networks have rendered it highly promising across a wide range of disease models. Its mechanism of action involves key signaling pathways and metabolic reprogramming, coupled with significant safety advantages, offering novel strategies for disease management.

In this study, we successfully established a sepsis model in male C57BL/6 mice using cecal ligation and puncture (CLP) surgery and systematically evaluated the effects of ART on renal function in these sepsis model mice. Additionally, we employed HK-2 cells to investigate the role of ART in sepsis-induced AKI. Subsequently, we utilized a multi-omics analysis strategy integrating metabolomics and transcriptomics to comprehensively analyze changes in metabolites and mRNA expression in mice kidney tissue following ART treatment, thereby revealing potential targets and molecular mechanisms underlying ART's efficacy in improving S-AKI. These findings not only provide new insights into the mechanisms by which ART treats S-AKI but also offer a scientific foundation for the clinical application of artemisinin-based drugs in managing this condition.

Materials and Methods

Animal Testing

Animal Handling

Male C57BL/6 mice (6–8 weeks) were obtained from Taizhou Huachuang Biotechnology Co., Ltd. (Jiangsu, China). All animals were housed under standard laboratory conditions with a 12-hour light/dark cycle and ad libitum access to food

and water. The environmental conditions were maintained at a constant temperature of 22.5 ± 2.5 °C and relative humidity of 50% ± 10%. The mice were acclimated for one week prior to the start of the experiment. All animal experiments were conducted in strict compliance with the Regulations and Ethical Guidelines for the Administration of Laboratory Animals of the People's Republic of China. The study protocol was reviewed and approved by the Institutional Animal Care and Use Committee (IACUC) of Zhuoqiang Biotechnology Institute (Protocol: ZQIA-2024-019).

A total of 25 male C57BL/6 mice were randomly divided into five groups (n=5 per group): Control group, CLP group, ART-L (75 mg/kg) group, ART-M (150 mg/kg) group, and ART-H (300 mg/kg) group. The 98% pure artesunate was procured from Yuan Ye Biology (batch number: M27IS216127). A stock solution of 100 mg/mL was prepared by dissolving 60 mg of ART in 600 μL of DMSO. Each mouse received a gavage volume of 500 μL. The dose and mode of administration for each group are presented in Table 1. Mice in the ART groups were pretreated with the corresponding doses of ART via gavage once daily for 5 days. The Control and CLP groups received 1% carboxymethyl cellulose (CMC) by gavage during this period. On day 6, AKI was induced by cecal ligation and puncture (CLP) surgery in the CLP and ART groups, while sham surgery was performed on the Control group. 1% pentobarbital sodium was administered intraperitoneally at a dose of 75 mg/kg body weight. After confirming successful anesthesia, the animal was secured on the operating table The surgical site was disinfected three times with a sterile cotton ball soaked in 75% alcohol. A 1-cm incision was made approximately 0.3 cm below the midpoint of the linea alba using surgical scissors, sequentially penetrating the skin, muscle layer, and peritoneum. Using flat forceps, the muscle layer was gently lifted to expose the abdominal cavity, and the cecum was carefully exteriorized. The cecum was ligated 1.6 cm from its distal end using a 4–0 suture, followed by two perpendicular punctures made with a 16-gauge needle. Immediately post-surgery, 50 mL/kg body weight of compound sodium chloride solution was subcutaneously injected into the neck and back region. The animal was subsequently returned to the cage, with water and food provided 4 hours later. Treatment with different concentrations of ART continued via intragastric administration once daily for 3 days post-surgery. The Control and CLP groups continued to receive 1% CMC by gavage. Blood samples were collected from the eye socket of each mouse, and serum was obtained by centrifugation. Kidneys were harvested for subsequent experiments.

Upon completion of drug administration in mice, the animals were euthanized, blood was collected via orbital sinus puncture, and the kidneys were dissected and rinsed with physiological saline. The left kidney was sectioned along the sagittal plane into two halves. A portion of the renal cortex was fixed in 2.5% glutaraldehyde, stored in the dark at 4°C for subsequent electron microscopy analysis. The remaining half of the left kidney was preserved in 4% formaldehyde at room temperature for hematoxylin and eosin (HE) staining. The right kidney was rapidly frozen in liquid nitrogen and subsequently stored at −80°C for further analysis.

Biochemical Experiments

Serum BUN and SCr levels in mice from each group were measured using a biochemical analyzer (Rayto Chemray, China). Working reagents were prepared according to the manufacturer's instructions, and the corresponding parameters were configured on the analyzer. Subsequently, samples were loaded into the system, and the analyzer automatically performed the measurements.

Table 1 The Administration Methods for C57BL/6 Mice

Group	−5d	0d	3d
Control	1%CMC, gavage, 1 time/d	Sham surgery	The same as operation
CLP	1%CMC, gavage, 1 time /d	CLP	−5d
CLP+ART (75mg/kg)	ART, gavage, 1 time /d	CLP	
CLP+ART (150mg/kg)	ART, gavage, 1 time /d	CLP	
CLP+ART (300mg/kg)	ART, gavage, 1 time /d	CLP	

HE Staining

Paraffin sections were prepared and rinsed with distilled water. The sections were stained with hematoxylin for approximately 2 minutes, followed by washing with distilled water until the tissues turned blue to purple. Differentiation was performed using 1% hydrochloric acid alcohol for 2 seconds. The sections were then washed again with distilled water until the tissues turned red, stained with eosin for 2–8 seconds, dehydrated with anhydrous ethanol, and cleared with xylene. Finally, the sections were sealed with neutral gum, observed under a microscope, and photographed.

Transmission Electron Microscopy

Kidney tissues were fixed in 1% osmium tetroxide for 2 hours, followed by washing with 0.1 M PBS 3–4 times (15 minutes per wash). Dehydration was performed using a graded ethanol series (30%, 50%, 70%, 80%, 90%, 95%, and 100%) for 15 minutes each. The tissues were then transferred to 100% acetone for 15 minutes, followed by 100% acetone containing anhydrous sodium sulfate for another 15 minutes. Next, the tissues were infiltrated with acetone-resin mixtures and subsequently replaced with pure resin overnight. After embedding, the samples were polymerized in a dry environment. Finally, the samples were ground and photographed.

Cell Experiment

Cell Culture and Treatment

LPS-induced inflammation and cell damage in HK-2 cells serve as cellular models of acute kidney injury (AKI).[30,31] HK-2 cells were obtained from Zhejiang Meisen Cell Technology Co., Ltd. (CTCC, catalog No. HCL-0150, Zhejiang, China) and cultured in DMEM medium supplemented with 10% fetal bovine serum (FBS) and 1% penicillin-streptomycin (P/S). The cells were divided into four groups: (1) Control group (HK-2), (2) LPS group (HK-2 + LPS, 100 μg/mL for 24 hours), (3) LPS + DMSO group (HK-2 + LPS, 100 μg/mL + DMSO), and (4) LPS + ART group (HK-2 + LPS, 100 μg/mL + ART, 10 μM for 24 hours). After incubation at 37°C in a 5% CO_2 incubator for 12 hours, 100 μg/mL LPS was added to the respective groups. For the DMSO group, an equivalent volume of DMSO was added to match the LPS concentration. The ART group received a final concentration of 10 μM ART after dilution in complete medium.

For the preparation of the ART stock solution, 83.33 mg of ART powder was accurately weighed and dissolved in 1 mL of DMSO to yield a 216.77 mM stock solution. For the LPS stock solution, 10 mg of LPS powder was accurately weighed and dissolved in 1 mL of PBS to prepare a 10 mg/mL stock solution. Following cell resuscitation, cells were centrifuged at 1200 rpm for 3 minutes, the medium was replaced with complete medium, and the cells were cultured at 37°C with 5% CO_2 for 24 hours. When the cell density reached 80%, the cells were digested with 0.25% trypsin, passaged, and adjusted to a density of 5×10^5 cells/mL. The cells were then seeded into 6-well plates (2 mL/well) and cultured in the incubator for an additional 24 hours. In the ART group, the ART stock solution was diluted with complete medium to achieve a final concentration of 10 μM. After culturing at 37°C with 5% CO_2 for 12 hours, LPS (100 μg/mL) was added to the culture medium. In the DMSO control group, an equivalent volume of DMSO was added, while in the negative control group, an equivalent volume of sterile PBS was added. The cells were subsequently cultured at 37°C with 5% CO_2 for an additional 24 hours before further analysis.

Determination of Cytotoxicity

Cytotoxicity was assessed using the Cell Counting Kit-8 (CCK-8) assay and the Annexin V-FITC/PI Apoptosis Detection Kit. Cell viability was measured using CCK-8 (CTCC, China). The cells were seeded in a 5% CO_2 incubator at 37°C and cultured for 24 hours before CCK-8 detection. Each well received 20 μL of CCK-8 solution and was incubated at 37°C in a 5% CO_2 incubator for 1–4 hours. The OD values were measured at 450 nm using a microplate reader, and the effect of the OD values on cell growth was analyzed. For apoptosis evaluation, the Annexin V-FITC/PI Apoptosis Detection Kit (BestBio, China) was used. Cells from each group were digested and collected using EDTA-free trypsin, washed with pre-cooled PBS, and resuspended in binding buffer. After adding 5 μL of Annexin V-FITC, the cells were incubated at room temperature for 15 minutes. Subsequently, 10 μL of PI staining solution was added, and the cells were incubated for

an additional 10 minutes at room temperature in the dark. Flow cytometry was performed for detection, and data were analyzed using FlowJo 7.6 software.

Biochemical Analysis

The levels of inflammatory factors, including TNF-α, IL-1β, and IL-6, in HK-2 cells from each group were measured using an ELISA kit (Elabscience, China). The copper content in HK-2 cells from each group was determined using reagents from Solarbio (China). The GSH levels in the cells were assessed using a GSH detection kit (Solarbio, China). After collecting the cell culture supernatant, centrifuge it at 1000×g for 20 minutes at 2–8°C to remove impurities and cellular debris. Collect the supernatant for subsequent analysis. Prepare the standard working solution by serially diluting the stock solution to a final concentration of 100 pg/mL. Set up standard wells, blank wells, and sample wells on the microplate. Add 100 μL of serially diluted standards to the standard wells, 100 μL of standard/sample diluent to the blank wells, and 100 μL of the test samples to the sample wells. Cover the microplate with an adhesive film and incubate at 37°C for 90 minutes. Add 100 μL of biotinylated antibody working solution to each well, re-cover the microplate, and incubate at 37°C for 1 hour. Wash the microplate three times by adding 350 μL of wash buffer to each well, soaking for 1 minute, and aspirating or flicking off the liquid. Add 100 μL of HRP-conjugate working solution to each well, re-cover the microplate, and incubate at 37°C for 30 minutes. Add 90 μL of substrate solution (TMB) to each well, re-cover the microplate, and incubate at 37°C in the dark for approximately 15 minutes. Terminate the reaction by adding 50 μL of stop solution to each well. Immediately measure the optical density (OD value) of each well at 450 nm using a microplate reader.

Transcriptome

Total RNA was extracted from liquid nitrogen-preserved tissues using the Qiagen RNeasy Mini Kit and assessed for purity and integrity using NanoDrop 2000 and Agilent 5400. Purified double-stranded cDNA was subjected to end-repair, A-tailing, and adaptor ligation. The resulting target double-stranded cDNA was amplified and purified by PCR to construct the sequencing library. Double-ended sequencing was performed on the Illumina NovaSeq PE150 platform. Raw data were filtered and quality-controlled using the default parameters of fastp software. After sequencing, raw data were processed to obtain clean data, which served as the basis for subsequent bioinformatics analysis.

Metabolome

Weigh 25 mg of the sample into an EP tube, add a homogenate bead, and add 500 μL of pre-cooled methanol-acetonitrile-water mixture. The target compound was chromatographically separated using a Waters ACQUITY UPLC BEH Amide column on a Vanquish (Thermo Fisher Scientific) ultra-high-performance liquid chromatograph. The original data were converted to mzXML format using ProteoWizard software, and metabolite identification was performed using the R package. The BiotreeDB (V3.0) database was utilized for metabolite annotation, followed by visual analysis using the R package.

Molecular Docking

The 2D structure of lactic acid was retrieved from PubChem, energy-minimized in Chem3D, and exported as mol2. The mol2 file was converted to pdbqt using AutoDockTools-1.5.7. Seven AMPK subunit proteins were identified in UniProt, and their lowest-resolution X-ray crystal structures were downloaded from PDB in PDB format. The A chains were isolated, water molecules removed, and structures optimized before importing into AutoDockTools-1.5.7 for charge neutralization, hydrogen addition, and removal of non-standard amino acids, then exported as pdbqt. Ligand-binding pockets were defined based on native ligand positions. Molecular docking between lactic acid and the seven AMPK subunits was performed using AutoDock Vina v1.1.2. Hydrogen bonds and hydrophobic interactions were visualized in 2D with LigPlot+ v2.2.9 and in 3D with PyMOL v3.1.1.

Western Blot

Protein lysates were prepared from 10 mg of tissue using ice-cold RIPA buffer with protease/phosphatase inhibitors. Samples were homogenized, centrifuged at 12,000 rpm for 20 min, and supernatants collected. Protein concentrations

were measured by BCA assay. Lysates were mixed with 5× SDS loading buffer, boiled for 5 min, and resolved on SDS-PAGE gels at 80 V (stacking) and 120 V (separation). Proteins were transferred to methanol-activated PVDF membranes (200 mA, 1–2 h), blocked with 5% BSA for 2 h, and incubated overnight at 4°C with primary antibodies. Membranes were washed with TBST, incubated with HRP-conjugated secondary antibodies (1:5000, 1 h at 37°C), and signals detected using ECL substrate and quantified via chemiluminescence imaging (Bio-Rad). β-actin served as the loading control. mTOR (2972S), p-AMPK (2535T), and AMPK (5832) antibodies were procured from Cell Signaling Technology (CST) and used at a dilution ratio of 1:1000. The p-mTOR (AF3308) antibody was obtained from Affinity Biosciences and applied at the same dilution ratio of 1:1000. LC3 (14,600-1-AP) and β-actin (66009-1-Ig) antibodies were acquired from Proteintech, with respective dilution ratios of 1:2000 and 1:150,000. Secondary antibodies, anti-rabbit IgG (ZB2301) and anti-mouse IgG (ZB2305), were sourced from Zhongshan Jinqiao Biotechnology (Beijing, China).

RT-PCR

Total RNA was extracted from 100 mg tissues using Lysis Buffer homogenization, chloroform phase separation, and silica-membrane purification, followed by ethanol washing and elution in RNase-free water. RNA quality was assessed by NanoDrop, showing A260/A280 ratios of 1.82–1.96 and concentrations of 171.67–195.27 ng/μL across groups. First-strand cDNA was synthesized using a reverse transcriptase kit under standard conditions (42°C for 40 min, 85°C for 5 min) with 5 μg RNA per 20 μL reaction. Target genes (LC3, mTOR, AMPK) and β-actin were amplified by SYBR Green-based qPCR using primers designed with Primer Premier 5.0. Each 20 μL qPCR reaction contained 10 μL 2 × Master Mix, 0.5 μM primers, and 1 μL cDNA template. Thermal cycling included 95°C for 10 min, followed by 40 cycles of 95°C for 20s, 55°C for 20s, and 72°C for 20s, with melt curve analysis from 60°C to 95°C. Data were normalized to β-actin using the $2^{-\Delta\Delta Ct}$ method, and amplification specificity was confirmed by single-peak melt curves and Ct values.

Statistical Methods

Statistical analyses were performed using GraphPad Prism 10.0 (GraphPad Software, San Diego, CA, USA). The Shapiro–Wilk test was conducted to assess the normality of the data, and Levene's test was employed to evaluate the homogeneity of variances. For datasets that met the assumptions of normality and homogeneity of variances, one-way ANOVA was used to compare means across multiple groups. In cases where these assumptions were not satisfied, the nonparametric Kruskal–Wallis test was applied to compare group medians. Results are presented as mean ± standard deviation (SD) for normally distributed data and as median (interquartile range) for non-normally distributed data. A p-value less than 0.05 was considered indicative of statistical significance.

Results

ART Improved Acute Kidney Injury in Sepsis Model Mice

To evaluate the pharmacological effects of ART, we first established an in vivo model and monitored the general condition of the mice. After 8 days of treatment, the body weight of the CLP group was significantly lower than that of the CON group, while the body weight of both the ART-M and ART-H groups was significantly higher compared to the CLP group (Figure 1A). The kidney index of the CLP group was significantly elevated relative to the CON group, whereas all ART-treated groups showed a significant decrease compared to the CLP group (Figure 1B). Additionally, we measured serum levels of renal function indicators, SCr and BUN. Results indicated that SCr and BUN levels were significantly higher in the CLP group compared to the CON group, while all ART-treated groups exhibited significantly lower Cr and BUN levels compared to the CLP group (Figure 1C and D). Based on these findings, the ART-H group demonstrated the most pronounced renal protective effect. To further assess the renal protective effects of ART, this study employed HE staining to examine histopathological changes in mice kidneys. Microscopic examination revealed that after modeling, the renal cortex structure became disordered, glomeruli were markedly shrunken, there was evident shedding of epithelial cells in the Bowman's capsule, extensive red blood cell extravasation, and inflammatory cell

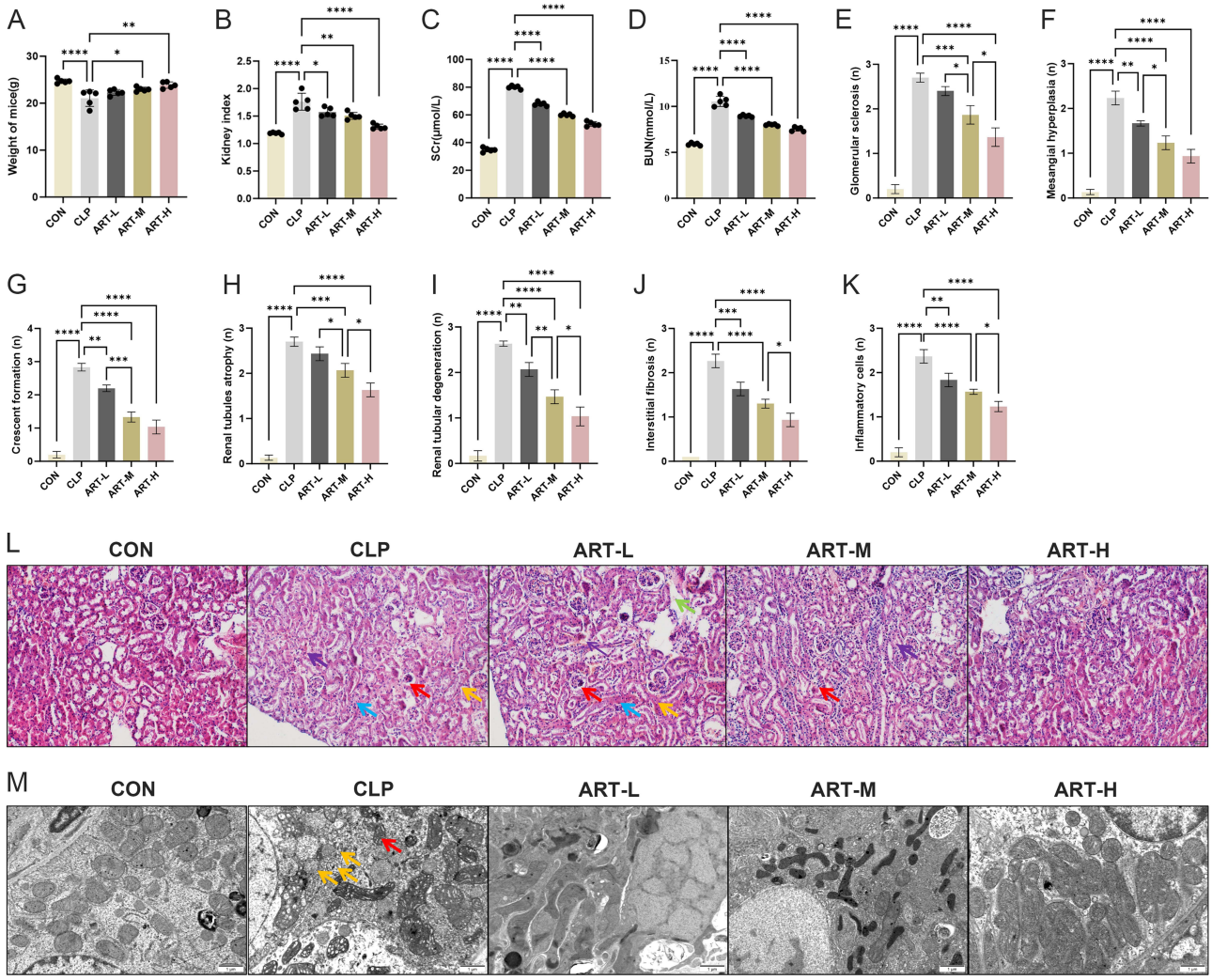

Figure 1 Pharmacodynamic assessment of ART in mice. (**A**) Body weight of mice. (**B**) Kidney index of mice. (**C** and **D**) The levels of SCr and BUN in the serum.(**E–K**) The scores of glomerular sclerosis, mesangial proliferation, crescent formation, renal tubular atrophy, renal tubular epithelial degeneration, interstitial fibrosis and inflammatory cell in each group in HE staining. (**L**) HE staining images of the kidney tissues. The red arrow indicates glomerular contraction, the yellow arrow indicates cortical structural disorder, the green arrow indicates epithelial cell shedding, the purple arrow indicates red blood cell exudation, and the blue arrow indicates inflammatory cell aggregation. (**M**) Electron microscope images of the kidney tissues. The red arrow indicates mitochondrial contraction, and the yellow arrow indicates an increase in lysosomes. Data are expressed as mean ± SD. **P* < 0.05, ***P* < 0.01, ****P* < 0.001, **** *P* < 0.0001.

infiltration in the renal interstitium. Post-treatment, these pathological changes were notably alleviated (Figure 1L). In addition, we performed a quantitative analysis of glomerular sclerosis, mesangial proliferation, crescent formation, tubular atrophy, tubular epithelial degeneration, interstitial fibrosis, and inflammatory cell infiltration in each group using HE staining. The results demonstrated that, compared with the normal group, the renal tissues in the model group exhibited significant pathological damage. After ART intervention, these damages were markedly alleviated, and the protective effect on renal tissues increased with higher concentrations of ART (Figure 1E–K). Electron microscopy was utilized to investigate the metabolic status and damage degree of kidney cells. Findings showed that post-modeling, numerous mitochondria were shrunken, and the number of autophagy lysosomes was significantly increased. Post-treatment, the extent of cellular damage was mitigated (Figure 1M).

ART Ameliorated Cell Injury on LPS-Treated HK-2 Cells

The LPS-induced HK-2 cell model serves as an in vitro platform for investigating S-AKI. HK-2 cells, which are a human renal tubular epithelial cell line, are frequently utilized in studies that simulate renal inflammation and injury. To assess

https://doi.org/10.2147/DDDT.S525701

the impact of ART intervention on LPS-induced acute kidney injury, an in vitro cell model was established. Initially, we measured the levels of renal inflammatory cytokines IL-1β, IL-6, and TNF-α across all groups. As anticipated, LPS treatment led to a significant increase in these cytokine levels. Notably, ART intervention significantly mitigated the LPS-induced elevation of renal inflammatory cytokines (Figure 2A–C). Subsequently, we examined the effect of ART on LPS-induced renal oxidative stress, focusing on the antioxidant GSH. Consistent with our hypothesis, GSH levels were markedly reduced following LPS treatment but were restored by ART intervention (Figure 2D). Furthermore, we investigated the influence of ART on LPS-induced cytotoxicity in HK-2 cells. CCK-8 assays revealed that LPS treatment significantly inhibited the proliferation of HK-2 cells, while ART intervention significantly reversed this inhibition (Figure 2E and F). Finally, apoptosis analysis demonstrated that LPS treatment promoted apoptosis in HK-2 cells, which was significantly attenuated by ART intervention (Figure 2G and H).

ART Alters the Metabolic Profiling in a Mice Model of Sepsis

To investigate whether ART can improve nephrotoxicity in a sepsis mouse model by modulating metabolism, this study examined metabolite changes in serum and kidney tissue samples across different groups. Metabolomics results are presented in Figure 3. Principal Component Analysis (PCA) revealed that the CON group and CLP group were completely separated in both serum and kidney samples. In tissue samples, while the CLP group and ART-H group did not show significant separation, their distribution trends differed (Figure 3A). Additionally, in serum samples, the

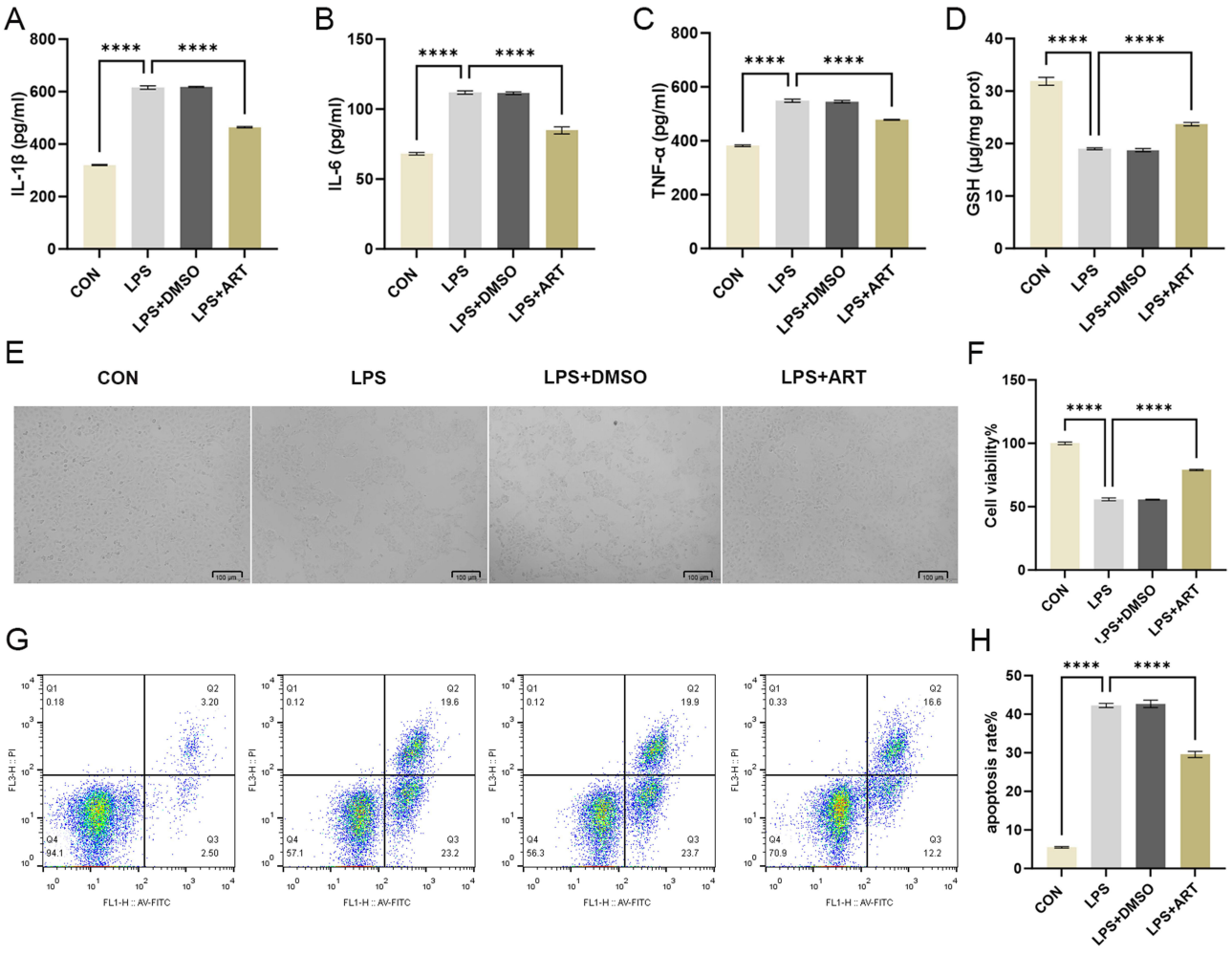

Figure 2 The impact of ART on LPS-treated HK-2 cells. (**A–D**) The levels of IL-1β, IL-6, TNF-α and GSH of each group. (**E** and **F**) CCK-8 assays depicting the degree of proliferation of each group. (**G** and **H**) The levels of cell apoptosis of each group. Data are expressed as mean ± SD. ****$P < 0.0001$.

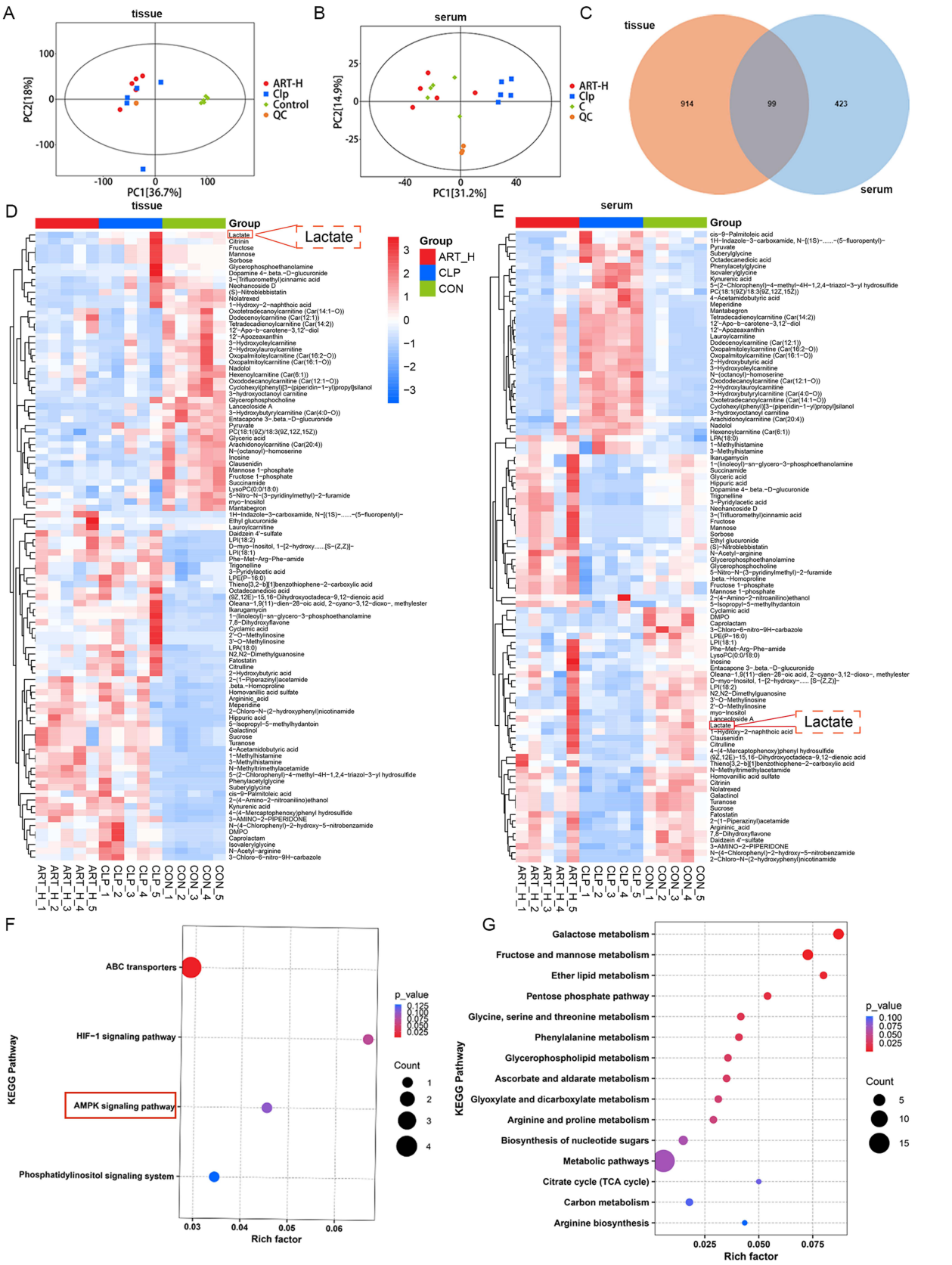

Figure 3 The integrated metabolite analysis of serum samples and kidney tissue samples. (**A** and **B**) PCA score plots for tissue metabolomics and serum metabolomics. (**C**) A comprehensive set of differentially expressed metabolites identified from serum and tissue samples across three groups (CON vs CLP vs ART-H). (**D**) Heat map for 99 differential metabolites in tissue. (**E**) Heat map for 99 differential metabolites in serum. The red boxes represent the differential metabolite lactate. (**F**) KEGG pathway of environmental information processing. The red box represents the AMPK signaling pathway in the enriched pathways. **G** KEGG pathway of metabolism.

https://doi.org/10.2147/DDDT.S525701

CLP group and ART-H group were distinctly separated (Figure 3B). A total of 1013 differential metabolites were identified among the three groups in tissue samples, 522 in serum samples, with 99 common differential metabolites shared between serum and tissue samples (Figure 3C). All differential metabolites met the significance threshold of $p < 0.05$. The heatmap illustrates the expression profiles of these differentially expressed metabolites across the three groups of tissues (Figure 3D). In addition, Figure 3E illustrates the variations in the levels of differential metabolites in serum across the three sample groups. KEGG enrichment analysis revealed that the primary signal transduction pathways involved were the HIF-1 signaling pathway and the AMPK signaling pathway (Figure 3F). Additionally, the predominant metabolic pathways encompassed carbohydrate metabolism and amino acid metabolism (Figure 3G). It is noteworthy that lactate, a metabolite associated with renal function, exhibited significant alterations in both serum and kidney tissue. Table 2 illustrates the levels of lactate changes in kidney tissue across the three groups of mice.

ART Alters the Transcriptomic Results in a Mice Model of Sepsis

To investigate the pathological mechanisms underlying ART treatment for S-AKI, mRNA sequencing was conducted on kidney tissues from each group of mice. PCA revealed distinct clustering patterns among the three groups, indicating significant differences (Figure 4A). The volcano plot demonstrated substantial alterations in mRNA expression between the CON and CLP groups, with a total of 4721 differentially expressed genes (DEGs); specifically, 1999 genes were upregulated and 2722 genes were downregulated. Furthermore, 1953 DEGs were identified between the CLP and ART-H groups, comprising 721 upregulated and 1232 downregulated genes ($p < 0.05$; Figure 4B). A clustering heatmap illustrated the expression changes of DEGs associated with the AMPK/mTOR signaling pathway (Figure 4C). The results demonstrated that, compared with the control group, genes including UIk2, Akt1s1, T61, Cab391, Strada, Mlst8, Rptor, Stradb, Mtor, and Deptor exhibited a downregulation trend in the CLP group. However, following ART intervention, the expression levels of these genes were reversed, showing an upregulation trend. Conversely, genes such as Stk11 and UIk1 were upregulated in the CLP group but exhibited downregulation after ART intervention. KEGG pathway enrichment analysis identified significantly enriched differential pathways, including key signaling cascades such as the mTOR signaling pathway and the AMPK signaling pathway (Figure 4D). Gene Ontology (GO) enrichment analysis elucidated the top 10 biological processes, cellular components, and molecular functions within each category (Figure 4E).

Combined Analysis of Metabolomics and Transcriptomics

To thoroughly investigate the pathological mechanisms of ART in treating S-AKI, we integrated metabolomics and transcriptomics data. Due to the large number of DEGs, we categorized these genes into up-regulated and down-regulated groups. Specifically, up-regulated genes are those that were down-regulated in the CLP group compared to the CON group but were up-regulated in the high-dose ART treatment group relative to the CLP group. Conversely, down-regulated genes are those that were up-regulated in the CLP group compared to the CON group but were down-regulated in the ART-H group relative to the CLP group. As shown in the Figure 5A and B, 33 pathways overlapped between the metabolomics data and both up-regulated and down-regulated gene sets respectively. Interestingly, among these shared pathways, the AMPK signaling pathway was significantly enriched (Figure 5C and D). Additionally, the mTOR signaling pathway emerged as a key pathway in the transcriptomic analysis. Given the well-established interplay between AMPK and mTOR signaling pathways in cellular energy metabolism, growth regulation, and autophagy, our findings suggest that the AMPK/mTOR axis may play a crucial role in the protective effects of ART against sepsis-induced AKI.

Table 2 The Variations in Lactate Concentrations Within Renal Tissues Across the Three Groups of Mice

Name	Formula	Class	Mean CON	Mean CLP	Mean ART-H	P-value
lactate	C3H6O3	Hydroxy acids and derivatives	420.78	468.99	250.74	<0.01

Note: The term Mean CON denotes the average lactate concentration in the control group, Mean CLP indicates the average lactate concentration in the model group, and Mean ART-H represents the average lactate concentration in the treatment group receiving a dosage of 300 mg/kg.

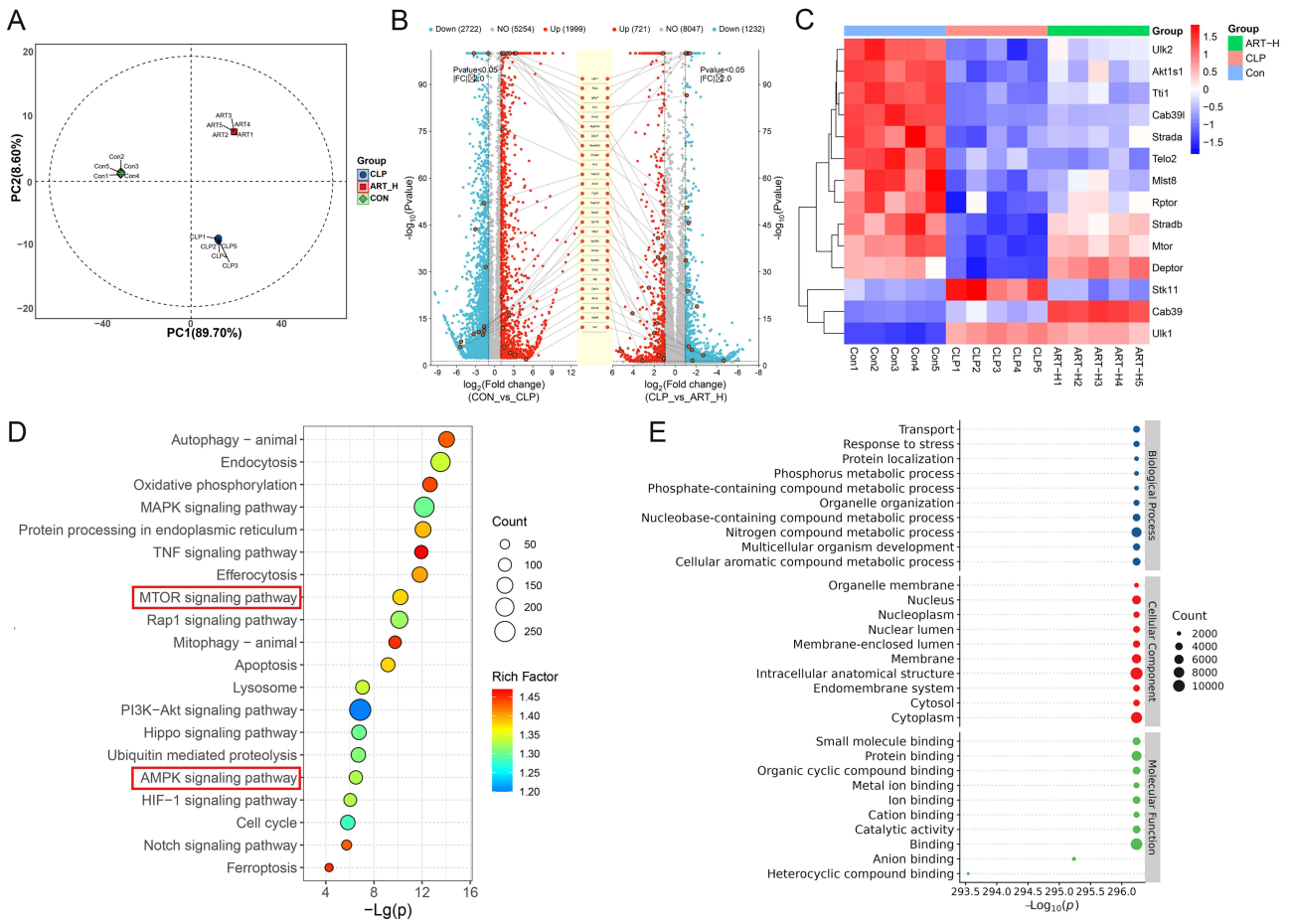

Figure 4 The transcriptomics analysis of kidney tissue samples. (**A**) PCA score plots of three groups. (**B**) Volcano map of CON vs CLP and CLP vs ART-H. **(C)** Heat map of differential expressed genes on the AMPK/mTOR pathway. (**D**) KEGG pathway enrichment analysis of the differentially expressed genes. The red box represents the AMPK and MTOR signaling pathway in the enriched pathways. (**E**) Biological process, cellular component and molecular function-based analyses of differential expression genes.

ART Affects the Expression of Target Molecule in the Lactic/AMPK/mTOR Pathway

To investigate the regulatory effect of ART on the lactic/AMPK/mTOR signaling pathway, this study employed Western blot and RT-PCR techniques to examine the phosphorylation levels of AMPK and mTOR, the protein expression of the autophagy marker LC3-II, as well as the dynamic mRNA expression of AMPK, mTOR, and LC3-II. Analysis of renal tissue revealed that compared with the normal control group, the model group exhibited significantly upregulated protein expression of p-AMPK and LC3-II (Figure 6C–F, $p < 0.0001$), while the protein level of p-mTOR was markedly inhibited (Figure 6E, $p < 0.0001$). Following ART intervention, all concentration groups effectively reversed these phenotypes: the protein expression of p-AMPK (Figure 6D) and LC3-II (Figure 6F) decreased in a dose-dependent manner ($p < 0.05$), whereas the protein level of p-mTOR was significantly restored (Figure 6E, $p < 0.01$). At the gene expression level, qPCR data were highly consistent with the protein results. Specifically, in the CLP model group, the mRNA levels of p-AMPK (Figure 6G) and LC3-II (Figure 6I) were significantly elevated ($p < 0.0001$), while the mRNA level of p-mTOR (Figure 6H) was significantly reduced ($p < 0.0001$). After ART treatment, the transcriptional levels of p-AMPK (Figure 6G, $p < 0.0001$) and LC3-II (Figure 6I, $p < 0.05$) were significantly downregulated, and the expression of p-mTOR mRNA was markedly enhanced (Figure 6H, $p < 0.05$). Further molecular docking analysis demonstrated that the binding energies of lactic acid with the AMPKα1 and AMPKγ1 subunits were −3.1 kcal/mol (Fig. 6A) and -4.2 kcal/mol (Figure 6B), respectively, suggesting that lactic acid may directly interact with and regulate the activity of the AMPK complex.

https://doi.org/10.2147/DDDT.S525701

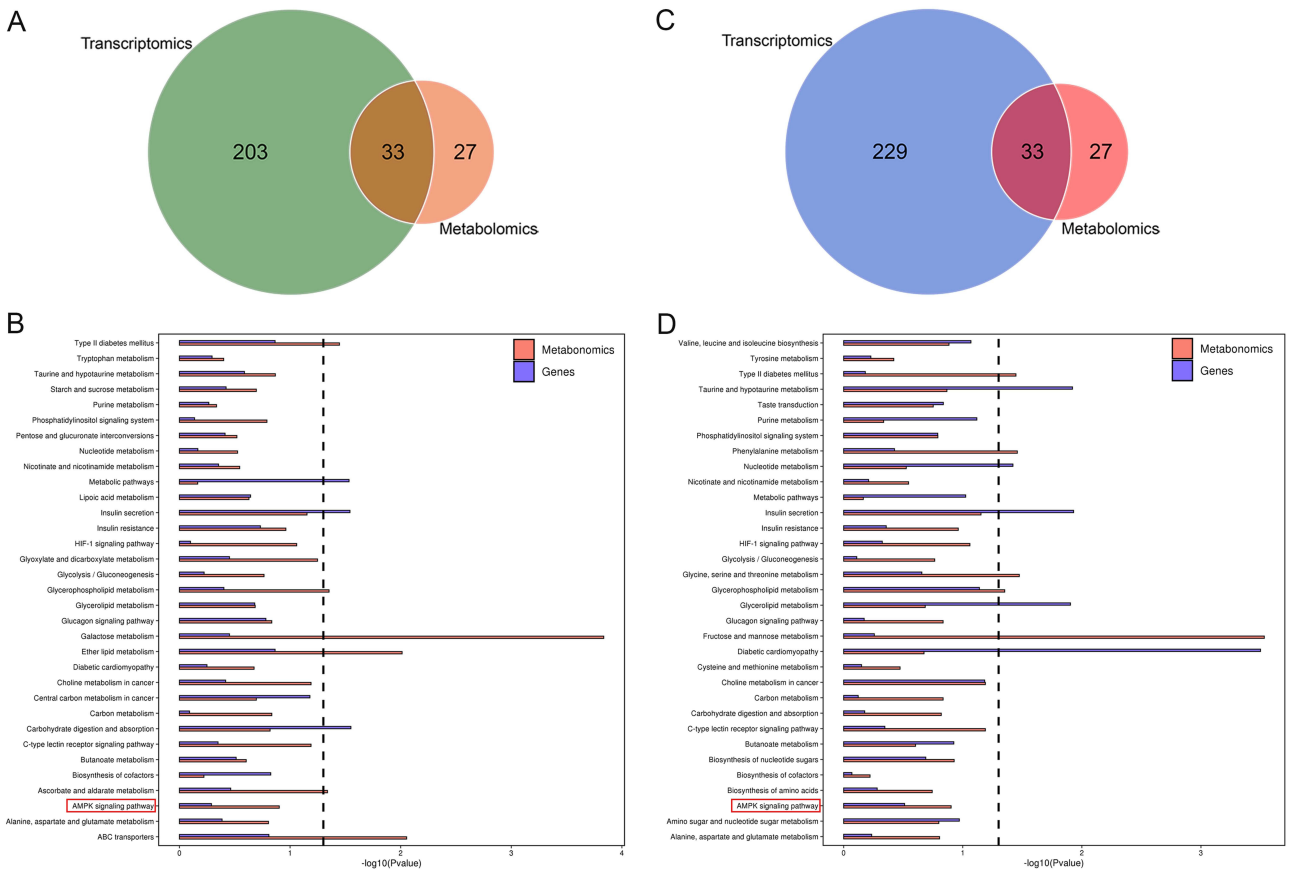

Figure 5 Results of joint analysis of metabolomics and transcriptomics. (**A**) KEGG pathway comparison Venn diagram of up-regulated gene. (**B**) KEGG comparison histogram of up-regulated gene. (**C**) KEGG pathway comparison Venn diagram of down-regulated gene. (**D**) KEGG comparison histogram of down-regulated gene. The red boxes in Figure 5B and D represent the AMPK signaling pathway in the intersection of the enriched pathways of the metabolome and transcriptome.

Discussion

Pharmacodynamic Evaluation of ART

Sepsis is a life-threatening multi-organ dysfunction syndrome resulting from the dysregulated host response to infection.[32] With the rising incidence of sepsis, its complications, such as S-AKI, have garnered increasing attention.[33] Recent studies have demonstrated that ART exhibit potential therapeutic effects on sepsis and its associated complications. For example, ART mitigates AKI by inhibiting necroptosis in macrophages and reducing inflammation in renal tubular epithelial cells.[34] Additionally, ART-nanoliposome-TPP, a novel mitochondria-targeted drug delivery system, alleviates cisplatin-induced AKI by suppressing oxidative stress and inflammatory responses.[17] These findings suggest that ART may represent a promising and effective therapeutic option for S-AKI. After 8 days of continuous administration, significant differences were observed in body weight and kidney index among the normal group, model (CLP) group, and ART-H group. Compared to the normal group, mice in the CLP group exhibited a marked decrease in body weight and a significant increase in kidney index. Conversely, mice in the ART-M and ART-H groups showed a significant recovery in body weight compared to the CLP group, while the kidney index in ART-treated groups was significantly lower than that in the CLP group. These findings suggest that ART can effectively mitigate weight loss and reduce renal edema in sepsis-induced mice. Additionally, renal function tests revealed that both serum creatinine (SCr) and blood urea nitrogen (BUN) levels were significantly reduced following ART treatment. Histopathological analysis demonstrated that ART intervention alleviated renal cortical structural disorganization, glomerular atrophy, Bowman's capsule epithelial cell shedding, erythrocyte extravasation, and renal interstitial inflammatory cell infiltration in CLP-induced mice. Electron microscopy further confirmed that ART treatment attenuated cellular damage, as evidenced by reduced mitochondrial shrinkage and decreased accumulation of autophagic lysosomes. Collectively, these results indicate that ART has the potential to improve renal function and reduce pathological damage in sepsis-associated acute kidney injury.

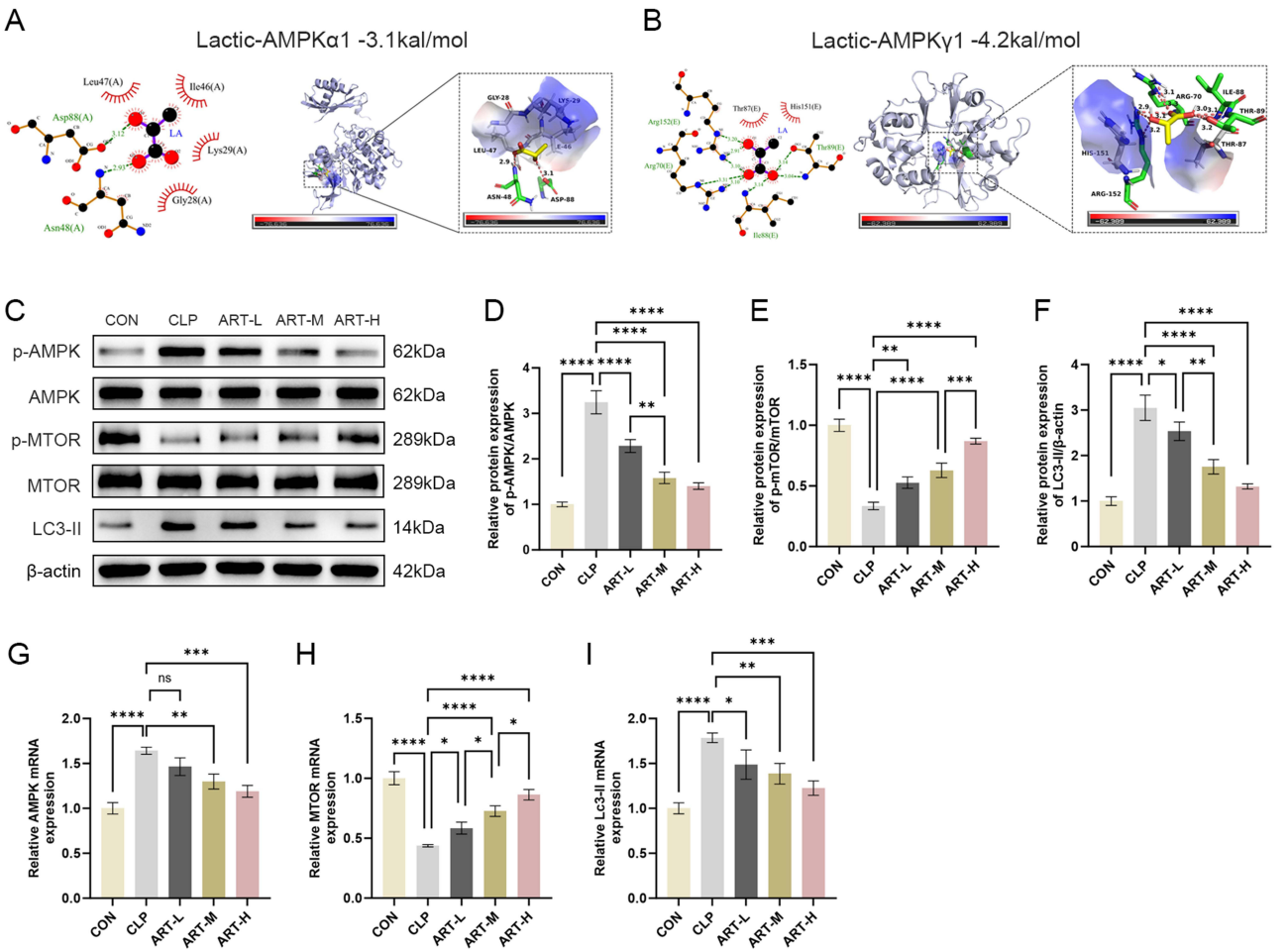

Figure 6 Relative expression of lactic/AMPK/mTOR pathway-related proteins and molecular docking. (**A and B**) The molecular docking results of lactic acid with AMPKα1 (PDB ID: 5ezv) and AMPKγ1 (PDB ID: 5iso). (**C–F**) The relative protein expressions of p-AMPK, p-mTOR, LC3-II in kidney tissues. (**G–I**) The relative mRNA expression levels of AMPK, mTOR, and LC3-II genes. Data are expressed as mean ± SD. **P* < 0.05, ***P* < 0.01, ****P* < 0.001, *****P* < 0.0001.

In addition, an LPS-induced S-AKI cell model was established to evaluate the effects of ART intervention on HK-2 cells. S-AKI is a common and severe condition in intensive care units (ICUs), with its pathogenesis closely linked to inflammatory responses.[35] Li et al demonstrated that blocking STAT3 with Stattic in a mouse model of LPS-induced AKI significantly reduced inflammation and fibrosis, decreased levels of inflammatory markers and extracellular matrix proteins, diminished macrophage infiltration, and modulated the expression of specific inflammation-related genes.[36] Consistent with the findings of this study, ART intervention significantly reduced the levels of IL-1β, IL-6, and TNF-α in the LPS-induced cell model. Moreover, GSH levels were markedly decreased following LPS induction but were restored after ART treatment. These results suggest that the inflammatory response plays a critical role in S-AKI, and inhibiting inflammatory signaling pathways or mitigating oxidative stress may represent effective therapeutic strategies for this condition. Additionally, CCK-8 assays and apoptosis analyses revealed that ART could significantly alleviate LPS-induced cytotoxicity in HK-2 cells. Specifically, ART treatment led to a significant increase in cell viability and a significant decrease in the apoptosis rate, indicating that ART has a potential protective effect against LPS-induced cellular inflammation and oxidative stress damage.

Metabolomics Elucidates the Metabolic Profile Alterations During ART Treatment for S-AKI

S-AKI is a common and severe complication in critical care medicine, characterized by a multifaceted pathogenesis.[37] Emerging evidence indicates that S-AKI not only stems from inadequate renal blood perfusion, microvascular dysfunction, and

https://doi.org/10.2147/DDDT.S525701

inflammatory responses but is also intricately linked to metabolic disturbances. Consequently, this study utilized metabolomics to elucidate the mechanisms through which ART exerts its protective effects against S-AKI.[38] This study found that inosine levels were significantly reduced in the CLP group and increased following ART intervention. Inosine, an important purine metabolite involved in energy metabolism and protein synthesis, has been shown to have multiple protective effects in AKI. Recent studies indicate that inosine can protect the kidneys from damage by inhibiting inflammatory responses and oxidative stress.[39] Moreover, inosine levels in the body are closely associated with renal function recovery, with urinary inosine concentrations positively correlated with creatinine clearance rate.[40] By participating in purine metabolism, inosine influences cellular energy supply and metabolic reprogramming.[41] In S-AKI, metabolic reprogramming is a critical pathological process, and inosine may promote renal cell survival and repair by modulating metabolic pathways. Notably, in this study, the lactate levels in the CLP group tended to increase compared to the CON group, while the ART-H group exhibited a significant reduction in lactate levels relative to the CLP group. The role of lactate in S-AKI has garnered increasing attention. Recent studies have demonstrated that lactate is not merely an end product of glycolysis but also exerts profound effects on cellular function and metabolic regulation through multiple mechanisms.[42] In AKI, lactate accumulation is closely associated with the reprogramming of energy metabolism in renal tubular epithelial cells.[43] Impaired mitochondrial function drives cells to shift from oxidative phosphorylation to enhanced glycolysis, thereby increasing lactate production.[44] A recent study revealed that under nutrient-depleted conditions, ULK1 enhances the enzymatic activity of lactate dehydrogenase A (LDHA) by phosphorylating its serine 196 residue, thereby promoting lactate production. Subsequently, lactate mediates the lactylation of type III phosphatidylinositol 3-kinase (Vps34) via the catalytic action of acyltransferase KAT5/TIP60. This lactylation significantly strengthens Vps34's interactions with Beclin1, Atg14, and UVRAG, and increases Vps34's lipid kinase activity, thereby promoting autophagy.[45] Therefore, ART intervention may protect renal function in patients with S-AKI by reducing intracellular lactate levels, inhibiting excessive autophagy, and mitigating inflammatory responses and oxidative stress.

Transcriptomics Analysis Reveals the Molecular Regulatory Network Governing ART Treatment for S-AKI

Metabolic profile changes often influence gene expression. Transcriptomics was employed to identify alterations in gene expression and to elucidate the potential molecular mechanisms underlying ART's improvement of S-AKI. Analysis revealed that, compared with the CON group, the CLP group exhibited 4721 differentially expressed genes (DEGs), including 1999 upregulated and 2722 downregulated genes. Additionally, 1953 DEGs were identified between the CLP and ART-H groups, comprising 721 upregulated and 1232 downregulated genes. KEGG analysis indicated that ART primarily affected the IFN signaling pathway, Rap1 signaling pathway, and mTOR signaling pathway. During AKI progression, these pathways regulate inflammation and oxidative stress, influencing kidney injury and repair. Specifically, IFN-β promotes cell polyploidy via the cGAS-STING pathway, exacerbating renal damage.[46] Rap1a activates the JAK2/STAT2 pathway, promoting inflammatory factor release and intensifying the inflammatory response.[47] The mTOR pathway regulates autophagy to mitigate inflammation and oxidative stress, protecting the kidneys from damage.[48] Modulating these pathways offers new targets and strategies for ART in treating S-AKI. Notably, the mTOR signaling pathway, crucial for cell growth, metabolism, and disease, consists of two complexes: mTORC1 and mTORC2. mTORC1 responds to nutritional, energy, and growth factor signals, promoting synthesis of proteins, lipids, nucleotides, and glucose while inhibiting protein degradation and autophagy.[49] In this study, mTOR expression was significantly reduced in the CLP group compared to the control group but was restored after ART intervention. The genes associated with the mTORC1 complex, including Deptor, mLST8, TELO2, and Tti1, exhibited significant changes following ART intervention. Meanwhile, ULK1 expression increased in the CLP group and decreased following ART treatment. These findings suggest that ART may alleviate autophagy in S-AKI by inhibiting the mTOR and activating ULK1.

Integrated Metabolomics and Transcriptomics Analysis Elucidates the Molecular Mechanisms of ART in Treating S-AKI

To elucidate the mechanisms by which ART mitigates renal injury and metabolic disturbances in S-AKI, we performed KEGG pathway analysis on differentially expressed metabolites and mRNAs identified through metabolomic and

transcriptomic profiling. The results revealed that the AMPK/mTOR signaling pathway is critically involved in the therapeutic effects of ART on S-AKI. As a central regulator of cellular energy metabolism and growth, the AMPK/mTOR pathway plays an essential role in maintaining cellular energy homeostasis and regulating autophagy.[50] AMPK functions as a cellular energy sensor, regulating energy metabolism in response to changes in the AMP/ATP ratio, whereas mTOR integrates signals from nutrients, energy status, and growth factors to control cell growth and autophagy.[51] In AKI, the dysregulation of the AMPK/mTOR pathway is closely related to renal injury.[52,53] The inflammatory response and metabolic disturbances induced by sepsis can lead to cellular energy metabolism impairments, which in turn activate AMPK to restore and maintain energy homeostasis.[54] However, excessive activation of AMPK may inhibit mTORC1, leading to hyperactivation of autophagy and consequently exacerbating damage to renal tubular epithelial cells.[54] In addition, inhibition of mTORC1 also reduces protein synthesis, thereby further impairing the cell's repair capacity.[48] Under conditions of energy deficiency, AMPK activation promotes glycolysis and increases lactate production. Accumulating lactate further impairs mitochondrial function, leading to a metabolic shift from oxidative phosphorylation to aerobic glycolysis, which may exacerbate renal injury.[55] In addition, lactic acid may also affect the activation of autophagy by regulating the AMPK/mTOR pathway.[56] Previous studies have shown that in Parkinson's disease, lactate enhances the activity of AMPK while inhibiting mTOR phosphorylation, thereby alleviating apoptosis in dopaminergic neurons.[57] Additionally, other research has indicated that lactate, acting as a metabolic regulator, activates AMPK, remodels the cellular metabolic profile, and consequently promotes the proliferation and differentiation of myoblasts.[58] When AMPK is activated, it inhibits mTORC1 by phosphorylating TSC2 and Raptor, thereby relieving the inhibition on the ULK1 complex and promoting autophagy.[59] The accumulation of lactic acid may modulate the degree of autophagy activation by regulating the AMPK/mTOR pathway, and excessive autophagy can further exacerbate renal cell damage. Therefore, ART may alleviate renal cell injury and improve S-AKI by reducing lactic acid levels, inhibiting excessive AMPK activation, thereby releasing mTORC1 inhibition, promoting ULK1 activation, and suppressing excessive autophagy.

Limitations and Future Perspective of This Study

There are several significant limitations to this study. First, while this study focused on major signaling pathways identified through omics analysis and explored the potential molecular mechanisms of ART in treating S-AKI, it did not verify key genes within these pathways at the molecular level. Secondly, signal transduction mechanisms are complex and influenced by multiple factors; however, this study did not conduct functional verification of the target genes. Therefore, future studies should employ RNA interference technology or relevant inhibitors to silence target genes at the cellular level, and use gene knockout techniques or inhibitors at the animal level to more comprehensively elucidate the molecular mechanisms by which ART improves S-AKI. Additionally, targeted metabolomics plays a crucial role in mechanism research. By providing precise qualitative and quantitative analysis, it offers important technical support and theoretical foundations for life science research, including exploring disease mechanisms, drug development and evaluation, and studying metabolic pathways and the relationship between metabolites and cell function. In future studies, we will concentrate on targeted metabolomics to further investigate the metabolism and distribution of ART in vivo. Finally, we will systematically evaluate the drug safety of ART to provide scientific evidence for its clinical application.

Conclusion

In this study, firstly, the potential protective effect of ART on S-AKI was explored in CLP-induced sepsis mouse model and LPS-induced HK-2 cell model. The results showed that ART could significantly improve the renal injury of septic mice, and also effectively reduce the degree of cell damage in HK-2 cells. Secondly, to elucidate the molecular mechanisms underlying the therapeutic effects of ART, an integrated metabolomics and transcriptomics approach was employed. The findings suggest that ART may mitigate inflammation and oxidative stress while improving renal function in S-AKI by modulating the lactate/AMPK/mTOR pathway and inhibiting excessive autophagy. This study provides a comprehensive understanding of the molecular mechanisms of ART in treating S-AKI, offering new theoretical insights and potential therapeutic strategies for clinical applications.

Data Sharing Statement

No datasets were generated or analysed during the current study.

Ethics Approval and Consent to Participate

The animal study was reviewed and approved by the Institutional Animal Care and Use Committee (IACUC) of Zhuoqiang Biotechnology Institute (ZQIA-2024-019).

Acknowledgments

We extend our appreciation to all the authors for their valuable contributions.

Author Contributions

All authors made a significant contribution to the work reported, whether that is in the conception, study design, execution, acquisition of data, analysis and interpretation, or in all these areas; took part in drafting, revising or critically reviewing the article; gave final approval of the version to be published; have agreed on the journal to which the article has been submitted; and agree to be accountable for all aspects of the work.

Funding

This work was supported by the Science and technology Research program of Henan Province (No: 242102310217) and the Joint Project of Henan Medical Science and Technology Project (No: LHGJ20230468).

Disclosure

The authors declare no competing interests in this work.

References

1. Guo J, Miao Y, Nie F, et al. Zn-Shik-PEG nanoparticles alleviate inflammation and multi-organ damage in sepsis. *J Nanobiotechnology*. 2023;21(1):448. doi:10.1186/s12951-023-02224-3
2. Prowle JRS-A-AKI. Sepsis-Associated AKI. *Clin J Am Soc Nephrol*. 2018;13(2):339–342. doi:10.2215/CJN.07310717
3. Kounatidis D, Vallianou NG, Psallida S, et al. Sepsis-associated acute kidney injury: where are we now? *Medicina*. 2024;60(3). doi:10.3390/medicina60030434.
4. Poston JT, Koyner JL. Sepsis associated acute kidney injury. *BMJ*. 2019;364:k4891. doi:10.1136/bmj.k4891
5. Bagshaw SM, Lapinsky S, Dial S, et al. Acute kidney injury in septic shock: clinical outcomes and impact of duration of hypotension prior to initiation of antimicrobial therapy. *Intensive Care Med*. 2009;35(5):871–881. doi:10.1007/s00134-008-1367-2
6. Bouchard J, Acharya A, Cerda J, et al. A prospective international multicenter study of AKI in the intensive care unit. *Clin J Am Soc Nephrol*. 2015;10(8):1324–1331. doi:10.2215/CJN.04360514
7. Rhee C, Jones TM, Hamad Y, et al. Prevalence, underlying causes, and preventability of sepsis-associated mortality in us acute care hospitals. *JAMA Netw Open*. 2019;2(2):e187571. doi:10.1001/jamanetworkopen.2018.7571
8. Chen L, Huang Q, Zhao T, et al. Nanotherapies for sepsis by regulating inflammatory signals and reactive oxygen and nitrogen species: new insight for treating COVID-19. *Redox Biol*. 2021;45:102046. doi:10.1016/j.redox.2021.102046
9. Zarbock A, Nadim MK, Pickkers P, et al. Sepsis-associated acute kidney injury: consensus report of the 28th acute disease quality initiative workgroup. *Nat Rev Nephrol*. 2023;19(6):401–417. doi:10.1038/s41581-023-00683-3
10. Legrand M, Bagshaw SM, Bhatraju PK, et al. Sepsis-associated acute kidney injury: recent advances in enrichment strategies, sub-phenotyping and clinical trials. *Crit Care*. 2024;28(1):92. doi:10.1186/s13054-024-04877-4
11. De Waele JJ, Girardis M, Martin-Loeches I. Source control in the management of sepsis and septic shock. *Intensive Care Med*. 2022;48(12):1799–1802. doi:10.1007/s00134-022-06852-5
12. Yao T, Su W, Han S, et al. Recent advances in traditional Chinese medicine for treatment of podocyte injury. *Front Pharmacol*. 2022;13:816025. doi:10.3389/fphar.2022.816025
13. Shi Q, Xia F, Wang Q, et al. Discovery and repurposing of artemisinin. *Front Med*. 2022;16(1):1–9. doi:10.1007/s11684-021-0898-6
14. Long Z, Xiang W, Xiao W, et al. Advances in the study of artemisinin and its derivatives for the treatment of rheumatic skeletal disorders, autoimmune inflammatory diseases, and autoimmune disorders: a comprehensive review. *Front Immunol*. 2024;15:1432625. doi:10.3389/fimmu.2024.1432625
15. Zhu M, Wang Y, Han J, et al. Artesunate exerts organ- and tissue-protective effects by regulating oxidative stress, inflammation, autophagy, apoptosis, and fibrosis: a review of evidence and mechanisms. *Antioxidants*. 2024;13(6):686. doi:10.3390/antiox13060686
16. Sun Z, Ma Y, Chen F, Wang S, Chen B, Shi J. Artesunate ameliorates high glucose-induced rat glomerular mesangial cell injury by suppressing the TLR4/NF-κB/NLRP3 inflammasome pathway. *Chem Biol Interact*. 2018;293:11–19. doi:10.1016/j.cbi.2018.07.011
17. Zhang J, Gu L, Jiang Y, et al. Artesunate-nanoliposome-TPP, a novel drug delivery system that targets the mitochondria, attenuates cisplatin-induced acute kidney injury by suppressing oxidative stress and inflammatory effects. *Int J Nanomed*. 2024;19:1385–1408. doi:10.2147/IJN.S444076

18. Koks G, Pfaff AL, Bubb VJ, Quinn JP, Koks S. At the Dawn of the transcriptomic medicine. *Exp Biol Med*. 2021;246(3):286–292. doi:10.1177/1535370220954788
19. Olivier M, Asmis R, Hawkins GA, Howard TD, Cox LA. The need for multi-omics biomarker signatures in precision medicine. *Int J Mol Sci*. 2019;20(19):4781. doi:10.3390/ijms20194781
20. Hrdlickova R, Toloue M, Tian B. RNA-Seq methods for transcriptome analysis. *Wiley Interdiscip Rev RNA*. 2017;8(1). doi:10.1002/wrna.1364
21. Yang W, Yin H, Wang Y, et al. New insights into effects of Kaixin powder on depression via lipid metabolism related adiponectin signaling pathway. *Chin Herb Med*. 2023;15(2):240–250. doi:10.1016/j.chmed.2022.06.012
22. Schrimpe-Rutledge AC, Codreanu SG, Sherrod SD, McLean JA. Untargeted metabolomics strategies-challenges and emerging directions. *J Am Soc Mass Spectrom*. 2016;27(12):1897–1905. doi:10.1007/s13361-016-1469-y
23. Liu C, Zhang C, He T, et al. Study on potential toxic material base and mechanisms of hepatotoxicity induced by Dysosma versipellis based on toxicological evidence chain (TEC) concept. *Ecotoxicol Environ Saf*. 2020;190:110073. doi:10.1016/j.ecoenv.2019.110073
24. Xu HH, Jiang ZH, Huang CS, et al. Global metabolomic and lipidomic analysis reveals the potential mechanisms of hemolysis effect of Ophiopogonin D and Ophiopogonin D' in vivo. *ChinMed*. 2021;16(1):3. doi:10.1186/s13020-020-00412-z
25. Li C, Li Y, Bai Z, Wang J, Li G, Xiao X. Herb induced liver injury by Xianling Gubao Tablets: a case assessed for causality using updated RUCAM and integrated evidence chain. *Chin Herb Med*. 2024;16(2):301–309. doi:10.1016/j.chmed.2023.10.005
26. Hu Y, Chen L, Zhao S, et al. Transcriptomics, proteomics, metabolomics and network pharmacology reveal molecular mechanisms of multi-targets effects of Shenxianshengmai improving human iPSC-CMs beating. *Clin Transl Med*. 2023;13(6):e1302. doi:10.1002/ctm2.1302
27. Zhang ML, Zhao X, Li WX, et al. Yin/Yang associated differential responses to Psoralea corylifolia Linn. In rat models: an integrated metabolomics and transcriptomics study. *ChinMed*. 2023;18(1):102. doi:10.1186/s13020-023-00793-x
28. Chen L, Wang J, Ren Y, et al. Artesunate improves glucose and lipid metabolism in db/db mice by regulating the metabolic profile and the MAPK/PI3K/Akt signalling pathway. *Phytomedicine*. 2024;126:155382. doi:10.1016/j.phymed.2024.155382
29. Guo X, Asthana P, Zhai L, et al. Artesunate treats obesity in male mice and non-human primates through GDF15/GFRAL signalling axis. *Nat Commun*. 2024;15(1):1034. doi:10.1038/s41467-024-45452-3
30. Zhang L, He S, Wang Y, et al. miRNA-20a suppressed lipopolysaccharide-induced HK-2 cells injury via NFκB and ERK1/2 signaling by targeting CXCL12. *Mol Immunol*. 2020;118:117–123. doi:10.1016/j.molimm.2019.12.009
31. Hu M, Wei J, Yang L, et al. Linc-KIAA1737-2 promoted LPS-induced HK-2 cell apoptosis by regulating miR-27a-3p/TLR4/NF-κB axis. *J Bioenerg Biomembr*. 2021;53(4):393–403. doi:10.1007/s10863-021-09897-1
32. Singer M, Deutschman CS, Seymour CW, et al. The third international consensus definitions for sepsis and septic shock (Sepsis-3). *JAMA*. 2016;315(8):801–810. doi:10.1001/jama.2016.0287
33. Mellhammar L, Wollter E, Dahlberg J, et al. Estimating sepsis incidence using administrative data and clinical medical record review. *JAMA Netw Open*. 2023;6(8):e2331168. doi:10.1001/jamanetworkopen.2023.31168
34. Lei XY, Tan RZ, Jia J, et al. Artesunate relieves acute kidney injury through inhibiting macrophagic Mincle-mediated necroptosis and inflammation to tubular epithelial cell. *J Cell Mol Med*. 2021;25(18):8775–8788. doi:10.1111/jcmm.16833
35. Nozaki Y, Hino S, Ri J, et al. Lipopolysaccharide-induced acute kidney injury is dependent on an il-18 receptor signaling pathway. *Int J Mol Sci*. 2017;18(12). doi:10.3390/ijms18122777.
36. Lee SH, Kim KH, Lee SM, et al. STAT3 blockade ameliorates LPS-induced kidney injury through macrophage-driven inflammation. *Cell Commun Signal*. 2024;22(1):476. doi:10.1186/s12964-024-01841-1
37. Peerapornratana S, Manrique-Caballero CL, Gómez H, Kellum JA. Acute kidney injury from sepsis: current concepts, epidemiology, pathophysiology, prevention and treatment. *Kidney Int*. 2019;96(5):1083–1099. doi:10.1016/j.kint.2019.05.026
38. Gómez H, Kellum JA. Sepsis-induced acute kidney injury. *Curr Opin Crit Care*. 2016;22(6):546–553. doi:10.1097/MCC.0000000000000356
39. Jackson EK, Kitsios GD, Lu MY, et al. Suppressed renoprotective purines in COVID-19 patients with acute kidney injury. *Sci Rep*. 2022;12(1):17353. doi:10.1038/s41598-022-22349-z
40. Hu T, Liu CH, Lei M, et al. Metabolic regulation of the immune system in health and diseases: mechanisms and interventions. *Signal Transduct Target Ther*. 2024;9(1):268. doi:10.1038/s41392-024-01954-6
41. Liu C, Wei W, Huang Y, Fu P, Zhang L, Zhao Y. Metabolic reprogramming in septic acute kidney injury: pathogenesis and therapeutic implications. *Metabolism*. 2024;158:155974. doi:10.1016/j.metabol.2024.155974
42. Li X, Yang Y, Zhang B, et al. Lactate metabolism in human health and disease. *Signal Transduct Target Ther*. 2022;7(1):305. doi:10.1038/s41392-022-01151-3
43. Kounatidis D, Tzivaki I, Daskalopoulou S, et al. Sepsis-associated acute kidney injury: what's new regarding its diagnostics and therapeutics? *Diagnostics*. 2024;14(24):2845. doi:10.3390/diagnostics14242845
44. Li H, Ren Q, Shi M, Ma L, Fu P. Lactate metabolism and acute kidney injury. *Chin Med J*. 2025;138(8):916–924. doi:10.1097/CM9.0000000000003142.
45. Sun W, Jia M, Feng Y, Cheng X. Lactate is a bridge linking glycolysis and autophagy through lactylation. *Autophagy*. 2023;19(12):3240–3241. doi:10.1080/15548627.2023.2246356
46. Zhang B, Zeng M, Li B, et al. Arbutin attenuates LPS-induced acute kidney injury by inhibiting inflammation and apoptosis via the PI3K/Akt/Nrf2 pathway. *Phytomedicine*. 2021;82:153466. doi:10.1016/j.phymed.2021.153466
47. Xu L, Zhang H, Wang Y, et al. FABP4 activates the JAK2/STAT2 pathway via Rap1a in the homocysteine-induced macrophage inflammatory response in ApoE(-/-) mice atherosclerosis. *Lab Invest*. 2022;102(1):25–37. doi:10.1038/s41374-021-00679-2
48. Shen SH, Wang RL, Yuan Q, et al. The roles of AMPK/mTOR autophagy pathway in the acute kidney injury-induced acute lung injury. *Chin J Physiol*. 2023;66(2):73–84. doi:10.4103/cjop.CJOP-D-22-00122
49. Levy T, Voeltzke K, Hruby L, et al. mTORC1 regulates cell survival under glucose starvation through 4EBP1/2-mediated translational reprogramming of fatty acid metabolism. *Nat Commun*. 2024;15(1):4083. doi:10.1038/s41467-024-48386-y
50. Yan LS, Zhang SF, Luo G, et al. Schisandrin B mitigates hepatic steatosis and promotes fatty acid oxidation by inducing autophagy through AMPK/mTOR signaling pathway. *Metabolism*. 2022;131:155200. doi:10.1016/j.metabol.2022.155200
51. Inoki K, Kim J, Guan KL. AMPK and mTOR in cellular energy homeostasis and drug targets. *Annu Rev Pharmacol Toxicol*. 2012;52:381–400. doi:10.1146/annurev-pharmtox-010611-134537

52. Zhou BY, Yang J, Luo RR, et al. Dexmedetomidine alleviates ischemia/reperfusion-associated acute kidney injury by enhancing autophagic activity via the α2-AR/AMPK/mTOR Pathway. *Front Biosci*. 2023;28(12):323. doi:10.31083/j.fbl2812323
53. Wang Y, Liu Z, Shu S, Cai J, Tang C, Dong Z. AMPK/mTOR signaling in autophagy regulation during cisplatin-induced acute kidney injury. *Front Physiol*. 2020;11:619730. doi:10.3389/fphys.2020.619730
54. Zhao W, Zhang L, Chen R, et al. SIRT3 protects against acute kidney injury via AMPK/mTOR-regulated autophagy. *Front Physiol*. 2018;9:1526. doi:10.3389/fphys.2018.01526
55. Aleidi SM, Al Fahmawi H, Masoud A, Rahman AA. Metabolomics in diabetes mellitus: clinical insight. *Expert Rev Proteomics*. 2023;20 (12):451–467. doi:10.1080/14789450.2023.2295866
56. Tan C, Gu J, Li T, et al. Inhibition of aerobic glycolysis alleviates sepsis-induced acute kidney injury by promoting lactate/Sirtuin 3/ AMPK-regulated autophagy. *Int J Mol Med*. 2021;47(3):19. doi:10.3892/ijmm.2021.4852
57. Li J, Chen L, Qin Q, et al. Upregulated hexokinase 2 expression induces the apoptosis of dopaminergic neurons by promoting lactate production in Parkinson's disease. *Neurobiol Dis*. 2022;163:105605. doi:10.1016/j.nbd.2021.105605
58. Zhou Y, Liu X, Huang C, Lin D. Lactate activates AMPK remodeling of the cellular metabolic profile and promotes the proliferation and differentiation of C2C12 Myoblasts. *Int J Mol Sci*. 2022;23(22):13996. doi:10.3390/ijms232213996
59. Jing Z, He X, Jia Z, Sa Y, Yang B, Liu P. NCAPD2 inhibits autophagy by regulating Ca(2+)/CAMKK2/AMPK/mTORC1 pathway and PARP-1/ SIRT1 axis to promote colorectal cancer. *Cancer Lett*. 2021;520:26–37. doi:10.1016/j.canlet.2021.06.029